

TAO, Vol.5, No.1, 91-107, March 1994

## Small-scale Plumes From a Semi-enclosed Basin: Yin-Yang Bay

CHUN-TE LIN<sup>1</sup>, KUANG-LUNG FAN<sup>1</sup> and SHENN-YU CHAO<sup>2</sup>

(Manuscript received 4 December 1993, in final form 18 March 1994)

### ABSTRACT

Sea-level elevation, offshore-current data and a sequence of color plume photographs were employed as a basis for numerical simulation of the unsteady behavior of small-scale plumes from Lien-Tong Stream which flows into Yin-Yang Bay located on the northeast coast of Taiwan. We first discuss how alongshore tides are affected by the irregular structure of the bottom topography and coastline in the studied area. Subsequently, tide-plume interaction is examined. The importance of tides on plumes can be estimated by a dimensionless tidal-excursion number,  $P = W/L$ , where  $W$  is the width of the source outlet and  $L$  is the tidal-excursion length. Most of the existing numerical models treat the case when  $P$  is large. In that case tidal effect is minor. In the present study  $P$  is  $O(1)$  or smaller; tidal advection becomes extremely important.

It is demonstrated numerically that the alongshore tides produce recirculation eddies inside the bay during both flood and ebb periods. The recirculation eddies induce plume movements inside the bay that are out of phase with the tidal currents over the shelf. Entering the coastal ocean, the plume water is advected by alongshore tides. The advection is rather asymmetric with respect to the axis of the bay due to the Earth's rotation. For the right-bound (ebb) tidal current, the plume tends to follow the Kelvin wave characteristic and hugs the coast. This tendency is absent during the left-bound (flood) tidal current. Scale analysis suggests that the advection by the ambient tidal current enhances this asymmetry.

(Key words: Tidal-excursion number, Recirculation eddies, Tide-plume interaction)

### 1. INTRODUCTION

Yin-Yang Bay, located on the northeast coast of Taiwan, is a small semi-enclosed basin with a 700-m wide mouth connecting to the northern shelf (Figure 1). The sea bed in the bay deepens northward to about 10-m near the mouth. Immediately offshore of the bay mouth is

---

<sup>1</sup> Institute of Oceanography, National Taiwan University, Taipei, Taiwan, R.O.C.

<sup>2</sup> Horn Point Environmental Laboratories, University of Maryland, Cambridge, Maryland, U.S.A.

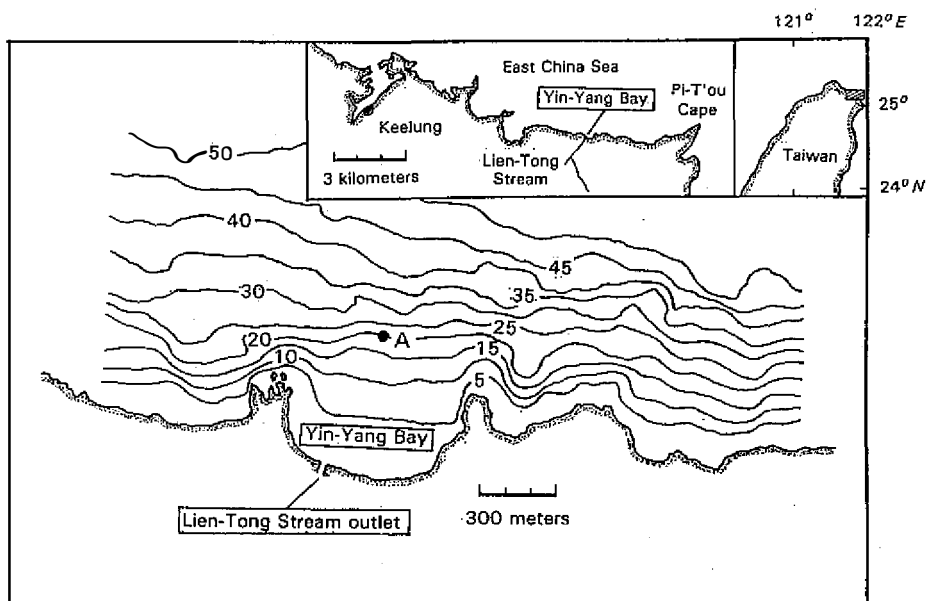


Fig. 1. Location, configuration and isobaths (in meters) of Yin-Yang Bay. Sea-level elevation data were collected at Keelung (see upper-right panels) and current data at station A.

the shelf/slope region, where the water depth increases from 10 to 40 m in less than 450 m. Inside the bay, the color photograph taken from a hill to the southwest of the bay showed that the river plume originating from Lien-Tong Stream has a distinctly yellow color, whereas the coastal water is between gray and blue (Figure 2). This stark color contrast was the main reason the bay was named "Yin-Yang". The yellow color of this surface plume comes from the suspended iron-oxide-coated clay colloidal particulates of Lien-Tong Stream (Yang *et al.*, 1990). Under normal conditions the iron will be removed as the particulates encounter high-PH coastal waters. The acidic waste water from Lien-Tong Stream lowers the PH value of coastal waters, allowing the iron-attached particulates to be carried afar. It was speculated that this mechanism is primarily responsible for the seaward dispersal of heavy metals (Pai *et al.*, 1990). Observed profiles of PH and salinity in the bay (Liang, 1989) suggest that the plume water is positively buoyant, despite the presence of suspended particles. Immediately adjacent to Lien-Tong Stream, the fresh and low-PH river water spreads seaward and over saline and high-PH coastal waters. Under calm conditions, the thickness of the surface plume was less than 2 m, characterized by an acidity of about 3 PH and a salinity of about 10 psu. Waters beneath the plume resemble coastal waters off the bay, with an alkalinity of 8 PH and a salinity of 30 psu. That the bottom water retains its offshore characteristics is a strong indication that the plume is positively buoyant.

Given a river width ( $W$ ) and an internal Rossby deformation radius ( $L_R$ ) characterizing the nearshore stratification, the importance of the Earth's rotation in modulating the plume can be measured by defining a Kelvin number,  $K = W/L_R$ . For  $K \geq 1$ , the Earth's rotation is important; the buoyant discharge spreads offshore from the source, turns anticyclonically, and upon reaching the coast forms a right-bound coastal current with a width scale comparable to  $L_R$  (Chao and Boicourt, 1986). For  $K \ll 1$ , the plume initially spreads out radially as

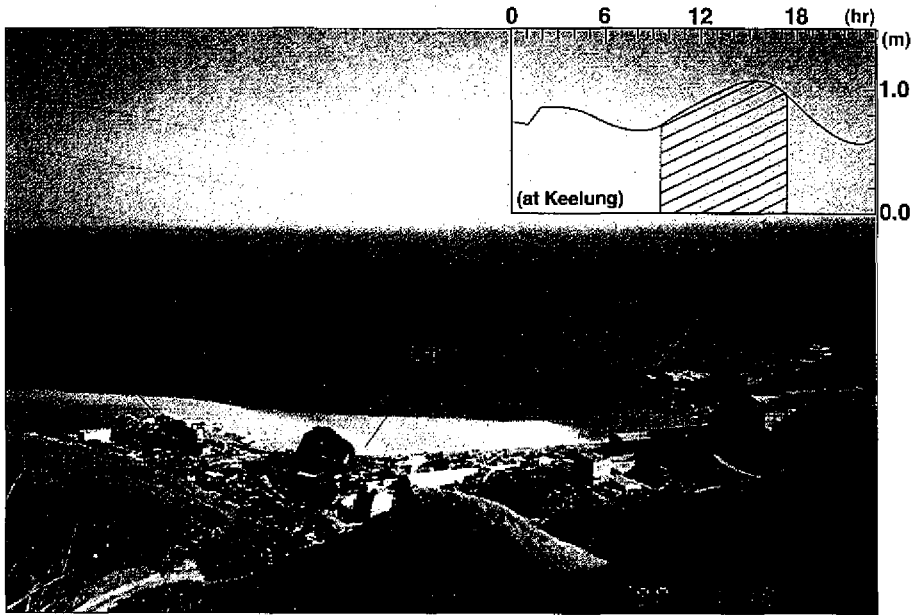


Fig. 2. Color photograph showing Lien-Tong Stream plume surrounded by the gray-blue coastal water (reproduced from Li *et al.*, 1991). The upper-right panel is the 1-day sea-level elevation curve in the studied area on January 18, 1990, with shading indicating the period monitored by photographs. R and L refer to the right and left capes bounding the bay, respectively. LT is the location of Lien-Tong Stream outlet.

in a nonrotating fluid. Upon reaching the radius  $L_R$ , a boundary current begins to form along the right-hand coast and near the perimeter of the plume, the appropriate time scale being  $O(f^{-1})$  where  $f$  is the Coriolis parameter (O'Donnell, 1990).

The effect of tides on plumes can also be estimated by defining a tidal-excursion number,  $P = W/L$ , where  $L$  is the tidal-excursion length. When  $T$  and  $V_0$  are the period and amplitude of tidal currents,  $L$  can be calculated as

$$L = \int_0^{T/2} V_0 \sin\left(\frac{2\pi t}{T}\right) dt = \frac{TV_0}{\pi} \quad (1)$$

For  $P \gg 1$ , the subtidal plume dynamics can only be modulated by the tidal residual eddies induced by the nonlinear transfer of vorticity from oscillating tidal currents to the mean field (Chao, 1990). As  $P$  decreases to unity or less, tidal effects become increasing advective and the plume is expected to oscillate with the tidal current. The Connecticut River plumes are notable examples (Garvine, 1974). The plumes emanating from Yin-Yang Bay have many features in common with the Connecticut River plumes in that the tidal effects are predominantly advective. With a characteristic semi-diurnal tidal current of 20 cm/sec, the tidal-excursion length off the bay is about 2.8 km, and  $P$  is less than a quarter. Whether

and how the Earth's rotation plays a role in modulating the tidally dominated plumes is a subject of the present numerical investigation.

The remainder of the paper is divided into four sections. An analysis of observations of the plumes in the bay is presented next. A description of a three-dimensional primitive equation model is given in section 3. In section 4 and 5 the numerical results follow. Section 6 summarizes and concludes this study.

## 2. OBSERVATIONS

The high visibility of the plumes enables us to identify the near-field distributions of plumes by employing a sequence of color photographs (taken from a nearby hilltop on January 18 1990). Sea-level elevation and current data were measured in December 1989. The current data were recorded at 5 m depth by deploying an Aanderaa RCM-7 current meter. The location of the station is shown in Figure 1 and is about 600 m seaward along the axis of the bay. The depth is approximately 20 m. Sea-level elevations were observed at Keelung, a city about 10 km west of the studied area (see Figure 1). Winds during the period photographs were taken were generally light and southerly (seaward). Consequently, coastal hills shield much of the bay and adjacent shelf from excessive wind forcing. Furthermore, as we shall see later, our numerical simulation seems able to explain most of the plume variabilities without invoking wind forcing. For these reasons the ensuing discussion excludes the wind. Hourly sea-level elevation data were furnished by Central Weather Bureau and others by the Institute of Harbour and Marine Technology.

During the winter of 1989-1990, tidal ranges were 0.5 m and 1.3 m in neap and spring periods respectively. On the average, tidal current had an amplitude of about 20 cm/sec. Subtidal mean current was extremely weak, generally less than 1 cm/sec. Spectral analysis of tidal elevations showed that the dominant tides had both diurnal and semi-diurnal components (Figure 3a), whereas the total energy spectrum of currents (Figure 3b) was dominated by the semi-diurnal component. Reduced diurnal contribution to currents may be caused by the strong bottom friction exerted by the complicated local bathymetries. Generally speaking, tides dominated the ambient current field off the bay.

Figure 4 is the hourly cross-correlation function of currents and sea-level elevations, with the convention that a positive lag indicates that the current is leading the sea level. The prevailing direction of currents was essentially alongshore. The elliptical curve covering nearly a 12-hour period indicates the domination of the semi-diurnal component. The largest correlation slightly exceeds 0.5; the imperfect correlation may be attributed to contributions by diurnal tides and other fluctuations. Furthermore, the maximum eastward current took place 4 hours after the high tide. In other words, the tidal current essentially flows eastward during ebb and westward during flood.

Figure 5 shows a sequence of aerial photographs taken 1~2 hours apart during the day on January 18, 1990. Also included on the upper-right panel of each photo is a 24-hour tidal-elevation curve under which the vertical line indicates the water level at the time the photograph was taken. The observational period covered the entire flood, high slack water and the first hour of ebb. The evolving plume underwent three stages of development.

### 2.1 Initial Flood

This stage is indicated by the first two photographs of the sequence. The river outflow was trapped near the stream outlet, and gradually expanded toward the north and east along the perimeter of the Bay. The northward expanding plume was quickly driven away westward

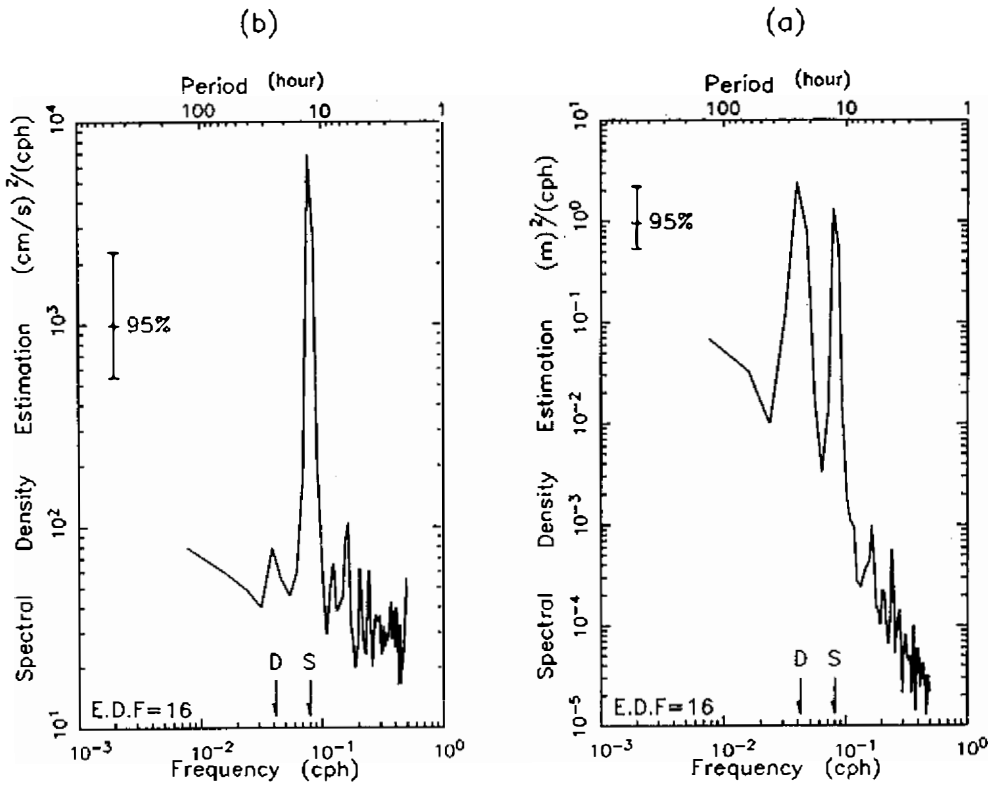


Fig. 3. Spectrum analyses of sea-level elevations and currents from December 3, 1989 to January 1, 1990, showing (a) spectral-density estimation of sea-level elevations, and (b) spectral-density estimation of currents. E.D.F., D, S and CPH represent equivalent degrees of freedom, diurnal, semi-diurnal and cycle per hour, respectively.

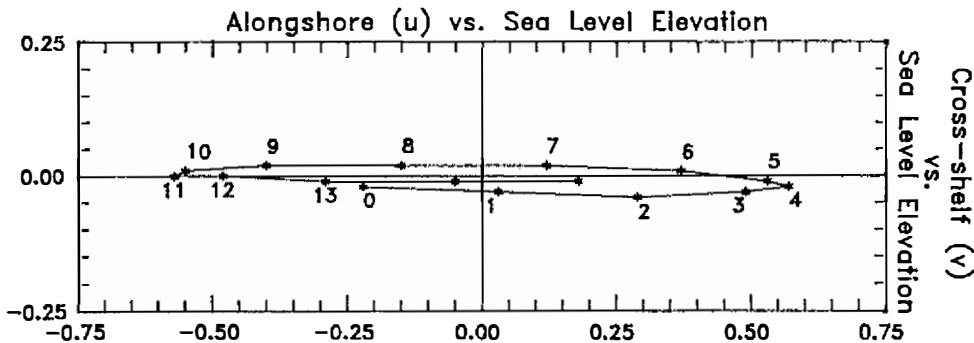


Fig. 4. The hourly cross-correlation function between currents and sea-level elevations with a positive lag indicating that currents lead sea-level elevations. Numbers by the stars represent the lag time in hours. Sea-level elevation and current data were from 18:00 Dec. 3 to 17:00 Dec. 7, 1989.

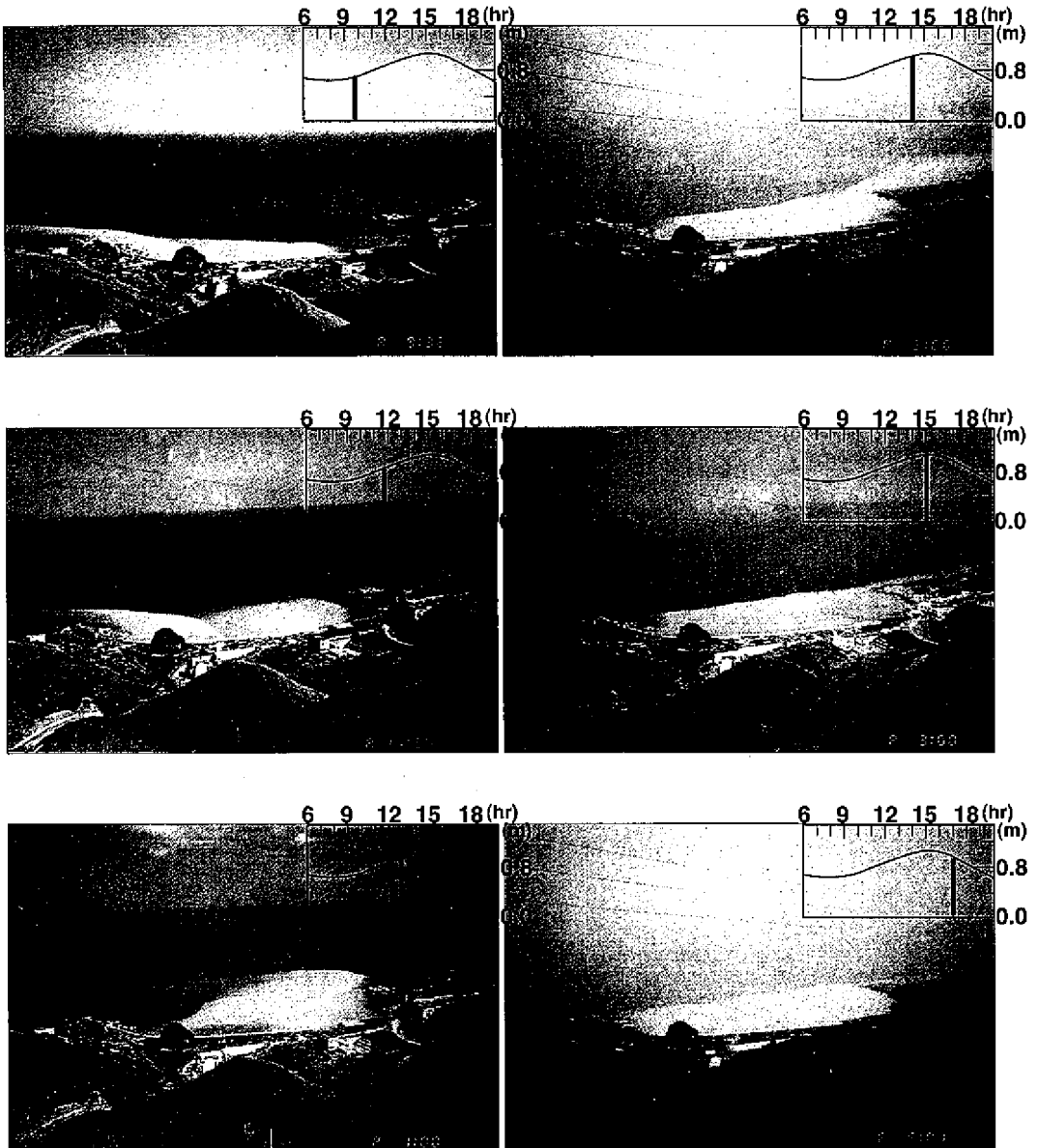


Fig. 5. The intratidal variability of the plume indicated by a series of photographs during the flood, high slack water and initial ebb from 09:32 am to 05:00 pm on January 18, 1990 (reproduced from Li *et al.*, 1991). Sea-level elevation for each snapshot is indicated on the upper-right panel of each photograph.

by the flood current as it reached the adjacent shelf near the left cape, leaving behind a trail of diluted plume water extending westward as seen in the upper left panels. Inside the bay, the plume continued to expand eastward toward the right cape of the bay.

## 2.2 Strong Flood

The flood current became strong at 01:00 pm. As shown in the third photograph of the sequence, the main body of the plume inside the bay extends northeastward, with the leading edge extending slightly beyond the right cape of the bay. A filament of much diluted plume water extends westward from the northwestern edge of the plume, apparently driven by the strong westward flood current.

## 2.3 High Slack Water

The last stage of the observations was made from 02:00 pm to 05:00 pm, covering the periods of weakening flood, high slack water and the first hour of ebb. Inside the bay, the plume was receding back toward the source area. The plume water flowing out of and beyond the right cape was diluted by the receiving water for lack of new supply of plume water from the bay. Being advected by the eastward tidal current, the faint trail of diluted plume water beyond the right cape seemingly approached the coast along its track eastward.

## 3. MODEL DESCRIPTION

The observed tidal currents were essentially alongshore. For cross-shelf tidal currents, realistic tides can be produced by imposing an oscillating current on the offshore boundary (Chao, 1990). The observed alongshore tides render this method ineffective. Instead, a tidal generating force will be imposed on the model ocean. Under the Boussinesq and hydrostatic approximations, the model ocean is governed by the following equations

$$\frac{Du}{Dt} - fv = -\frac{1}{\rho_0}P_x + F + A_M \nabla^2 u + \nu u_{zz} \quad (2a)$$

$$\frac{Dv}{Dt} - fu = -\frac{1}{\rho_0}P_y + G + A_M \nabla^2 v + \nu u_{zz} \quad (2b)$$

$$P_z = -g\rho \quad (2c)$$

$$\frac{DS}{Dt} = A_H \nabla^2 S + kS_{zz} \quad (2d)$$

$$u_x + v_y + w_z = 0 \quad (2e)$$

where  $(u, v, w)$  are velocities in the  $(x, y, z)$  directions,  $\rho$  is the density,  $\rho_0$  a reference water density,  $S$  the salinity,  $D/Dt$  is a nonlinear operator such that  $D\sigma/Dt = \partial\sigma/\partial t + \partial(u\sigma)/\partial x + \partial(v\sigma)/\partial y + \partial(w\sigma)/\partial z$ ,  $A_M$  and  $\nu$  are the horizontal and vertical mixing coefficients for momentum,  $A_H$  and  $k$  the horizontal and vertical mixing coefficients for salt. The water density is related to temperature and salinity by Eckart's (1958) rational approximation

under one atmospheric pressure. For simplicity, the temperature is fixed at 15°C, so that  $\rho$  is only a function of salinity.

Tidal generating forces,  $F$  and  $G$ , are assumed to be barotropic with diurnal and semi-diurnal components, and are given as

$$F = \sum_{j=1}^2 |\bar{F}_j| \cos(\omega_j t + \arg(\bar{F}_j)) \quad (3a)$$

$$G = \sum_{j=1}^2 |\bar{G}_j| \cos(\omega_j t + \arg(\bar{G}_j)) \quad (3b)$$

Their amplitudes and phases,  $(\bar{F}_j, \bar{G}_j)$  are related to the observed tidal currents by using one-dimensional linear shallow water equations which neglect horizontal free-surface gradient terms. Each Fourier component,  $(\bar{F}_j, \bar{G}_j)$ , can be given as

$$\bar{F}_j = (i\omega_j + \varepsilon)\bar{u}_j - f\bar{v}_j \quad (4a)$$

$$\bar{G}_j = (i\omega_j + \varepsilon)\bar{v}_j + f\bar{u}_j \quad (4b)$$

where  $\varepsilon$  is the Rayleigh friction coefficient chosen as  $2.5 \times 10^{-5} \text{ sec}^{-1}$ ,  $j=1$  or 2 represents respectively diurnal and semi-diurnal components,  $(\bar{u}_j, \bar{v}_j)$  are Fourier coefficients of currents estimated from observed current data off the bay,  $\omega_j = 2\pi/T_j$  is the frequency of component  $j$  with  $T_1=24$  hours and  $T_2=12$  hours. The following parameters, used throughout the study, are estimated from 4-day current data from 18:00 Dec. 3 to 17:00 Dec. 7, 1989:

$$|\bar{F}_1| = 1.1452 \times 10^{-4} \text{ cm/sec}^2$$

$$\arg(\bar{F}_1) = 81.82^\circ$$

$$|\bar{F}_2| = 1.8154 \times 10^{-3} \text{ cm/sec}^2$$

$$\arg(\bar{F}_2) = 45.22^\circ$$

$$|\bar{G}_1| = 9.026 \times 10^{-5} \text{ cm/sec}^2$$

$$\arg(\bar{G}_1) = 2.33^\circ$$

$$|\bar{G}_2| = 8.286 \times 10^{-4} \text{ cm/sec}^2$$

$$\arg(\bar{G}_2) = -42.27^\circ$$

Tidal currents produced by eq. (3) are compared with those observed in Figure 6, with top and bottom panels corresponding to alongshore and cross-shelf components, respectively. In general, the reconstituted tides reproduce the observed alongshore currents reasonably

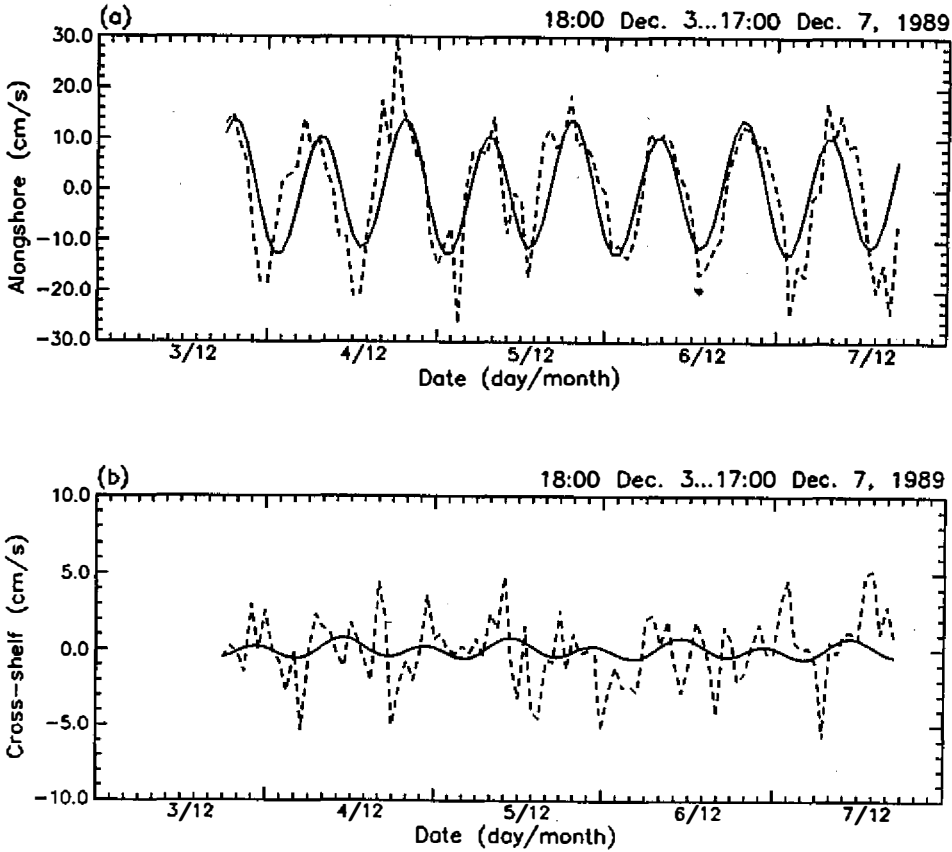


Fig. 6. The series of observed tidal currents (broken lines) and reconstituted tidal currents from equations (3) (solid lines). (a) alongshore ( $u$ ) component, positive eastward; (b) cross-shelf ( $v$ ) component, positive northward.

well. Percentagewise, the cross-shelf currents are not reproduced very well. Since the cross-shelf tidal currents are much weaker than the alongshore tidal currents, this deviation is not serious.

The irregular bottom topography and coastline can act as a catalyst to induce nonlinear transfer of vorticity from the oscillating tidal field to the mean field. Thus, realistic basin geometry and bottom topography are employed in the vicinity of the bay. Figure 7 shows the plane view of the model basin. The ocean is assumed to be cyclic in the alongshore  $x$ -direction, and the cyclic condition is given as follows

$$\phi_{1,j} = \phi_{N-1,j} \quad (5a)$$

$$\phi_{N,j} = \phi_{2,j} \quad (5b)$$

where  $\phi$  denotes sea level, salinity or currents, and  $N$  the maximum number of grids in the  $x$ -direction. In the  $y$ -direction, the ocean is bounded to the north by a zonal wall and to the

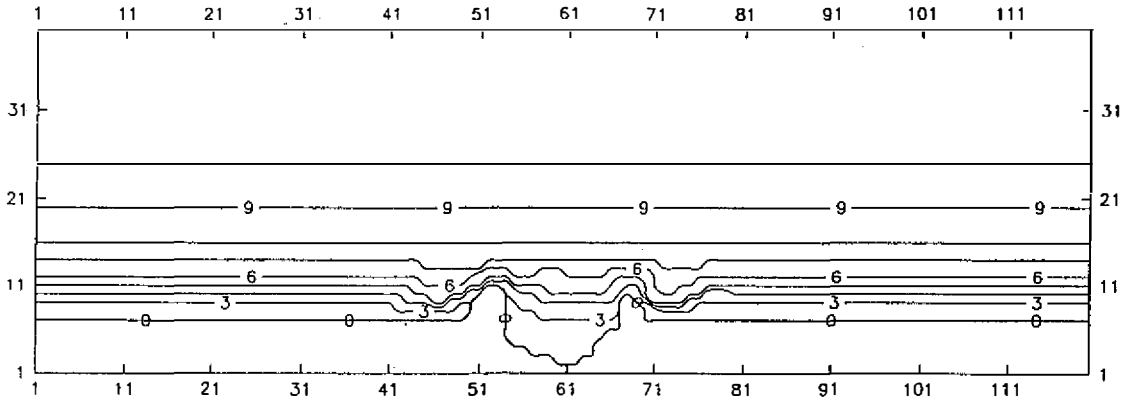


Fig. 7. The model geometry and isobaths expressed in number of vertical layers and contoured from 0 (land) to 10 (50-m depth) at intervals of 1 layer. The minimum model depth is 4-m, equivalent to 2 layers between contour 0 and 3. Otherwise, the number of layers between two contours is equal to the contour value of the southern one. The domain size is 6 km in the alongshore direction and 2 km in the cross-shelf direction. Horizontal scales are in units of  $\Delta x$  (= 50 m).

south by the irregular coastline. On the northern boundary, we specify zero currents and 35 psu salinity boundary conditions, and also zero sea-level gradient to avoid water setup. The solid southern boundary is impenetrable, no slip and impermeable,

$$(u, v) = (0, 0) \quad (6a)$$

$$\frac{\partial S}{\partial n} = 0 \quad (6b)$$

where  $n$  is normal to the boundary. The model's horizontal resolution is 50 m in  $x$  and  $y$  directions. There are ten levels in the vertical; the top five being 2 m thick, followed by two 5 m and three 10 m grid spacings, yielding a maximum 50 m depth offshore. The water depth gradually reduces to a minimum of two levels along the coast. Finer resolution near the surface is meant to better resolve shallow features nearshore. East and west of the bay, isobaths and coastlines are idealized to be zonal to preserve the cyclic condition in the alongshore direction.

Vertical boundary conditions are the following. On the free surface,  $z = \eta$ ,

$$\frac{\partial S}{\partial z} = 0 \quad (7a)$$

$$v \frac{\partial(u, v)}{\partial z} = (0, 0) \quad (7b)$$

$$\frac{\partial \eta}{\partial t} + \frac{\partial U}{\partial x} + \frac{\partial V}{\partial y} = 0 \quad (7c)$$

where  $(U, V)$  is vertically integrated flow in the  $x$  and  $y$  directions. On the variable bottom,  $z = -H(x, y)$ ,

$$\frac{\partial S}{\partial z} = 0 \quad (8a)$$

$$w = -uH_x - vH_y \quad (8b)$$

$$\nu \frac{\partial(u, v)}{\partial z} = b(u^2 + v^2)^{1/2}(u, v) \quad (8c)$$

where  $b$  is a dimensionless drag coefficient. The river mouth of Lien-Tong Stream, with  $2\Delta x$  width, is located at the southwestern corner of the bay. The buoyancy forcing is imposed in conjunction with no slip condition by specifying  $S=15$  psu for the two-level depth. The model ocean is spun up from rest, assuming the initial salinity is 35 psu everywhere. The governing equations (2) subject to boundary conditions, (5)-(8), are center-differenced in space and time to second-order accuracy. The numerical code is a generalization of the general circulation model developed by Semtner (1974) to allow for a free surface (see Chao and Paluszkiwicz, 1991). Barotropic and baroclinic solutions are resolved with time steps  $\Delta t$  and  $\Delta T$ , respectively. The following parameters are used throughout this study:

$$\Delta T = 12 \text{ sec}$$

$$\Delta t = 0.3 \text{ sec}$$

$$A_M = 5000 \text{ cm}^2/\text{sec}$$

$$A_H = 500 \text{ cm}^2/\text{sec}$$

$$\nu = k = 1 \text{ cm}^2/\text{sec}$$

$$b = 0.002$$

$$f = 6.192 \times 10^{-5} \text{ sec}^{-1}$$

Note that  $A_H$  is 10 times smaller than  $A_M$  in order to avoid excessive smoothing of plume features. The experiment is divided into two stages. The first is to spin up tidal currents for 3 semi-diurnal tidal cycles for the purpose of establishing quasi-equilibrium tidal currents. Thereafter, the buoyancy forcing from Lien-Tong Stream is imposed and maintained constant until the end of the third day.

#### 4. TIDAL CURRENTS

Figure 8 shows eight sequential snapshots of surface tidal currents covering a 12-hour tidal cycle starting at 23:00 on December 4, 1989. By imposing the barotropic tidal generating force, the interior tidal currents show essential characteristics similar to those observed off the bay. Modulated by the minor diurnal tidal component, the maximum flood current (22 cm/sec) at 02:00 is 7 cm/sec faster than the maximum ebb current at 08:00. As suggested by observations, tidal currents over the shelf are basically alongshore. The turning of tides is a bit earlier nearshore than offshore. Since the tidal currents are primarily alongshore, there is little shoaling in the cross-shelf tidal currents.

Near the embayment, effects of coastline geometry and bottom topography produce eddies. The shoaling bottom topography near capes and the headland itself accelerate the incoming alongshore flow, enhancing the downstream advection of vorticity which is generated by side-wall friction or horizontal gradient of bottom friction. The strengthened flow entering the lee region decelerates due to the increasing water depth. The import of vorticity from the upstream region will be trapped in the lee of capes, producing lee eddies alternating in sign with sizes comparable to the tidal-excursion length. With 4 cm/sec characteristic tidal velocity in the bay, the tidal-excursion length is about 550 m and the tidal-excursion number will be on the order of unity locally. A detailed description of the physical process producing tidal eddies can be found in Zimmerman (1981). In Figure 8, the tidal current field contains two cyclonic eddies during flood and two anticyclonic eddies during ebb in the lee of two capes. Because the flood current is stronger than the ebb current, cyclonic eddies are displaced farther downstream of the capes than anticyclonic eddies. Of particular relevance to the nearfield plume variabilities are the eddies inside the bay because they produce currents opposite to the prevailing tidal currents over the shelf.

How the eddies inside the bay develop in time can be elaborated as follows. Initially the beginning flood current gradually flows into the bay along the left coast of the right cape. As the flood current strengthens, the inflow location moves westward and becomes separated from the cape, eventually reaching about the center of the mouth of the bay to produce a cyclonic eddy field in the bay. The eddy is maintained until the beginning of the ebb. Thereafter an anticyclonic eddy begins to develop near the left cape of the bay in a similar fashion, and continues until the start of the next flood, completing the tidal cycle.

#### 5. TIDE-PLUME INTERACTION

Small streams intruding into receiving waters initially behave as jets in nonrotating fluids; the Earth's rotational effect sets in at a distance sufficiently away from the source. One notable example is the unsteady buoyant jet formed by the low-salinity tidal outflow from Leschenault estuary into the higher-salinity Koombana Bay, Western Australia (Luketina and Imberger, 1987). Very near the source, the initial momentum flux forms a well-mixed turbulent jet attached to the bottom. Slightly away, buoyancy dominates the momentum of the discharge and the weakened jet becomes a radially-spreading buoyant surface plume separating from the bottom. There the vertical entrainment becomes important. Beyond this field the intensity of the currents grows on available potential energy and therefore is not very sensitive to the strength of the inflow (Chao and Boicourt, 1986). Our interest is well beyond the flow field very near to the source; the river forcing is modeled as a buoyancy

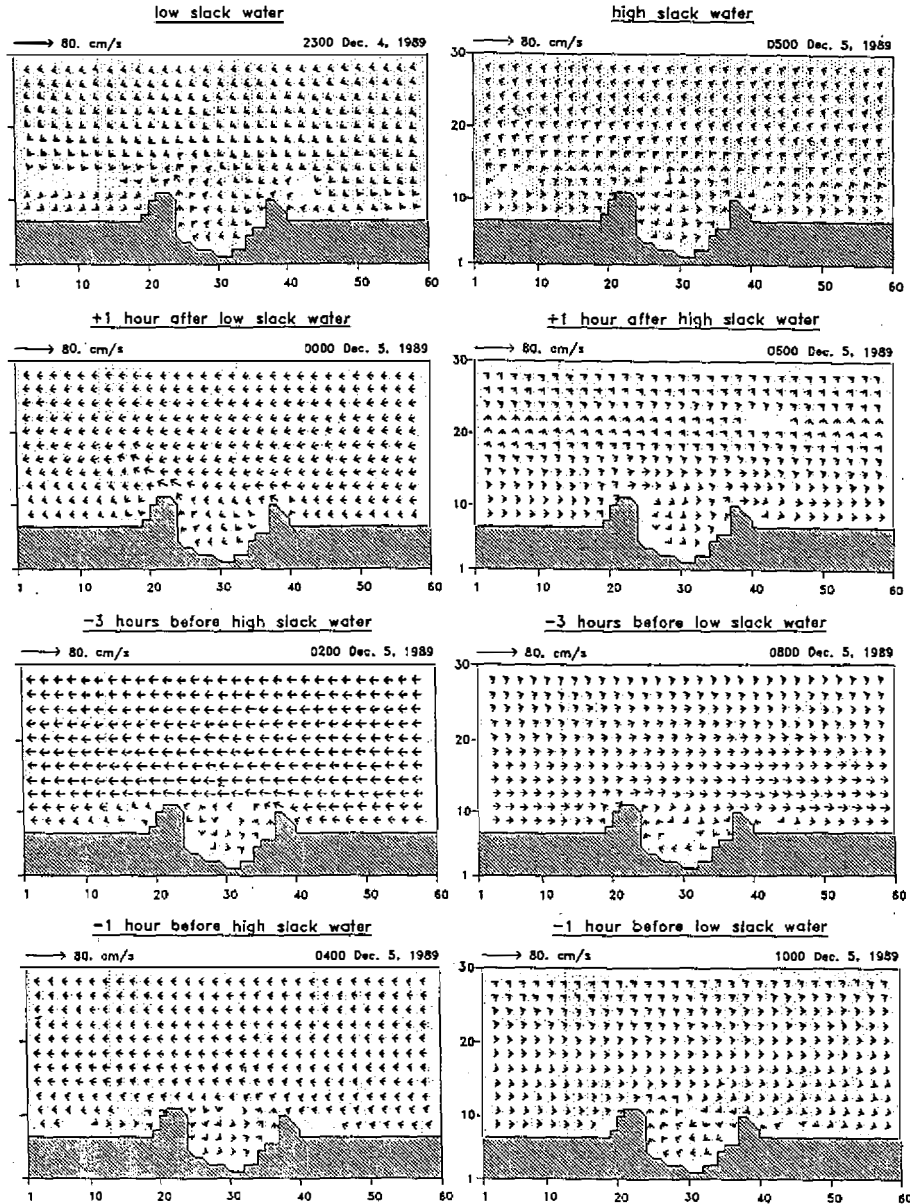


Fig. 8. Intratidal variability of surface-flow fields during one 12-hour tidal cycle after one day of tidal forcing over the model basin. Left panels: from low slack water to flood period. Right panels: from high slack water to ebb period. Horizontal scales in units of  $\Delta x$ .

source without initial momentum flux. Additionally, the river forcing has been initiated at different phases of the dominant tidal cycle. The conclusion is qualitatively the same as that of the ensuing experiment. Due to the shortage of manpower, the lack of concurrent tidal-current measurement during January 1990 is unfortunate. Here we make a simplifying assumption that the essential diurnal and semi-diurnal tidal characteristics as inferred from December 1989 data remained the same in January 1990 and therefore can be used for the January 1990 numerical simulation. It should be noted, however, that other tidal constituents may interfere with diurnal and semi-diurnal tides on longer time scales. This uncertainty notwithstanding, our numerical simulation does reproduce the observed intratidal variability of the plume reasonably well, lending support to our modeling strategy.

Figure 9 shows eight sequential snapshots of surface flow and salinity fields starting from 09:00 on January 18, 1990. The buoyancy forcing was imposed at 20:00 on January 17, 13 hours before the first snapshot. Compared to Figure 5, Figure 9 shows characteristics similar to the observed features. At the initial flood stage, the frontal boundary is much sharper on the upstream side than on the downstream side with respect to the flood current. Entering the shelf, the plume is deflected to the west due to the westward crossflow. As the flood current strengthens at 11:00 and 12:00 on January 18, the plume water inside the bay expands eastward toward the right cape in a fashion similar to that of the observed plume. The onshore flow near the left cape, being part of the cyclonic eddy inside the bay, separates the plume water inside the bay from that offshore, and in the process allows for a greater percentage of plume water to expand eastward inside the bay. Within the bay, the counterclockwise expansion of the plume is further enhanced by the cyclonic eddy. Concurrently, the outgoing plume water is swept away by the strong westward tidal current. At high slack water, 15:00 on January 18, and the initial ebb tidal phase, the cyclonic eddy has completely separated the plume inside the bay from that swept afar and the much-reduced body of the plume water is narrowly oriented toward the northeast, debouching onto the adjacent shelf. As the ebb current strengthens, plume detachment over the shelf and the plume expansion inside the bay proceed in directions opposite to those during the flood period, again in qualitative agreement with observations (Figure 5). For the ebb current, an anticyclonic eddy inside the bay drives the nearfield plume variability instead.

Comparing the snapshot at 11:00 with that at 17:00, the far-field dispersal of the plume waters off the bay is asymmetric with respect to the axis of the bay. The dispersal to the east during the ebb period is much closer to the shoreline than that to the west during the flood period. The asymmetry is apparently caused by the Earth's rotation and was observed earlier off the Connecticut River mouth (Garvine, 1974). Previous theoretical models (Matsuno and Nagata, 1987; O'Donnell, 1990; etc.) suggested that the effect of planetary rotation exerts only secondary influence on the unsteady behavior of small-scale plumes. The numerical study of gravity currents in a rotating channel (Wang, 1985) revealed that the time scale for the formation of baroclinic boundary currents bounded to the right by a coast is on the order of half inertial period, about 14 hours for the latitude of 25.124°N. By comparison, the effect of the Earth's rotation sets in much earlier in the present model. In the present environment with tidal-excursion number ( $P$ ) less than unity, the development of internal Kelvin waves along the coast will be accelerated by the effect of an eastward (ebb) current. Simple scale analysis will show that the relation between the relevant time scale with the mean current ( $T_1$ ) and that without the mean current ( $T_0$ ) should be given as

$$T_1 = T_0 \left( \frac{U_0}{c} + 1 \right)^{-1} \quad (9)$$

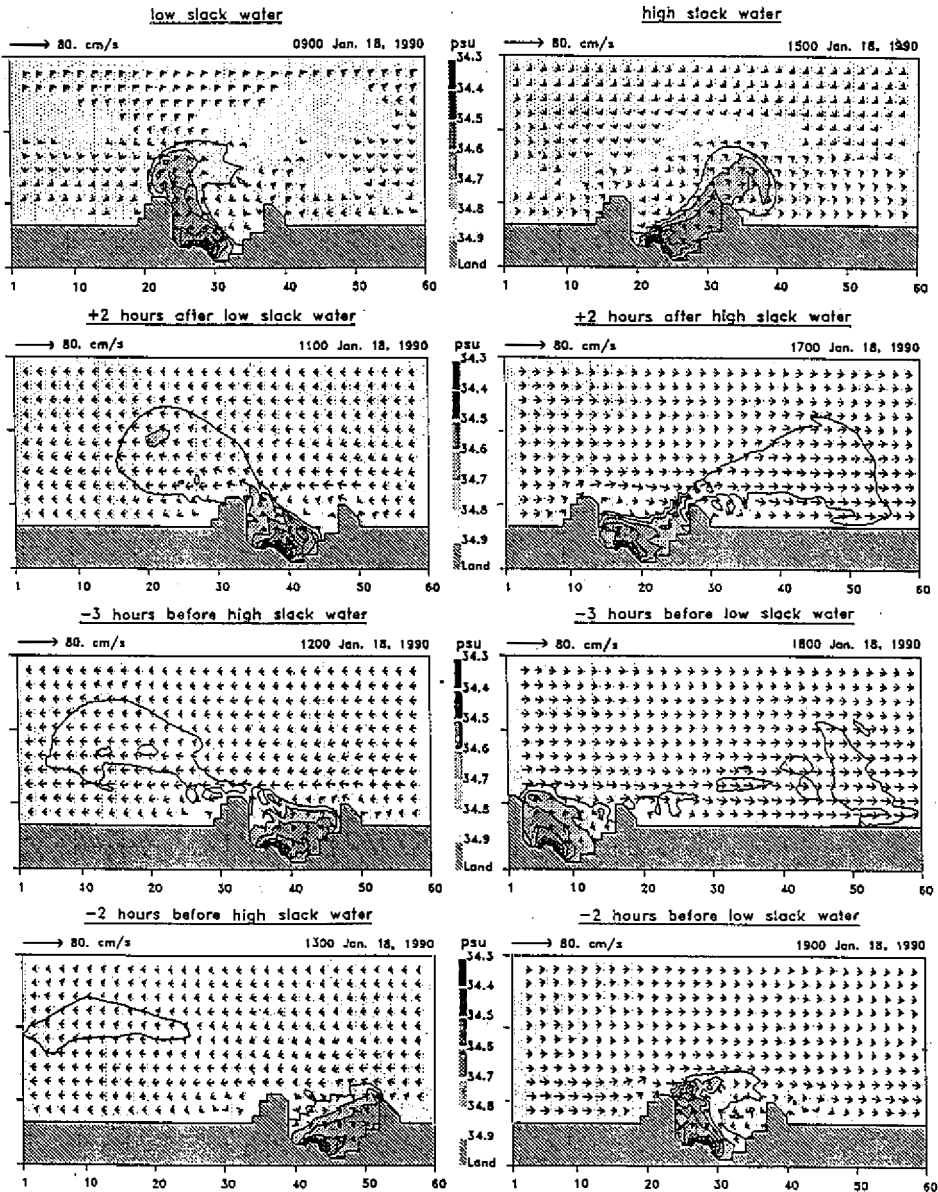


Fig. 9. Plane views of surface flow and salinity fields during a tidal cycle after 13 hours of buoyancy forcing initiated at 04:00 on the second day of tidal forcing. Left panels: from low slack water to flood periods. Right panels: from high slack water to ebb periods. The corresponding simulation time on January 18, 1990 is shown on top of each panel. Salinity contours in psu at intervals of 0.1 psu. Alongshore scale in units of  $\Delta x$ .

where  $U_0$  is the speed of the mean current and  $c$  the phase speed of internal Kelvin waves. Here the appropriate  $U_0$  and  $c$  are 20 and 5 cm/sec, respectively;  $T_1$  will be less than 3 hours during the ebb tide, about 5 times shorter than that without the mean current.

## 6. SUMMARY AND CONCLUSIONS

The model can be improved in many ways, among which the foremost is how tides are incorporated. In a limited area model, tides can be included through either a tidal generating force or a boundary forcing. The latter practice usually requires knowledge of the spatial distribution of tidal characteristics on all boundaries, which is wanting. This is the main reason a tidal generating force is employed in this work. One interesting feature borne out by this practice is the development of reverse flows in the bay against the tidal generating force during both flood and ebb periods, suggesting that recirculation eddies in the bay are remotely forced. Further improvement may be made by resolving  $M_2$ ,  $S_2$ ,  $K_1$  and  $O_1$  tides. Such a practice is not taken here because improving temporal resolution but not spatial resolution of tides is not likely to bring the model closer to reality. Even with one semi-diurnal and one diurnal component, our best fit indicates that the former dominates the latter. It can be said that the modeled plume is essentially driven by one component of semi-diurnal tides. This maximum simplification seems adequate to explain intratidal plume variabilities on short time scales, but is apparently ill-suited for longer periods of simulation.

The model can also be improved by removing the offshore wall to allow for incorporation of remote forcings from the open ocean. Its effects on plumes and tides can be assessed as follows. Based on nearshore and offshore depth scales, the external Rossby radii of deformation are about 100 and 350 km, respectively. Both are more than one order-of-magnitude larger than the basin size. Thus the model essentially precludes external Kelvin waves that are of large-scale origin. Baroclinically, the characteristic depth and salinity deficit of the plume over the shallow shelf are about 2 m and 0.1 psu, respectively. The internal Rossby radius nearshore is therefore about 400 m, or five times smaller than the cross-shelf basin scale. There is no density stratification and therefore no baroclinic Rossby radius near the offshore wall. Thus, the offshore wall should not affect the development of baroclinic Kelvin waves nearshore.

By including the tidal and river forcings over the realistic bathymetry and shoreline geometry, the foregoing numerical simulation has replicated some of the salient features of the observed plume variabilities in and out of Yin-Yang bay. In keeping with the observations, the modeled plume movement inside the bay is out of phase with tidal currents offshore, and owes its existence to the tidally induced eddies inside the bay. Over the shelf, plume disperses in the direction of tidal-currents. During the ebb tide, the eastward dispersing plume tends to hug the coast to its right, apparently following the direction of Kelvin waves. This also agrees with the limited observations available so far.

The rather significant asymmetry in the far-field plume dispersal induced by the Earth's rotation is an unexpected result that calls for attention. The dominant flood and ebb periods last for only 6 hours each, seemingly too short for the Earth's rotational effect to set in. Yet a baroclinic right-bound current is set up during the ebb period in a few hours. It is suggested that the eastward ebb current significantly accelerates the development of Kelvin-like waves, a process that is likely applicable to most small-scale plumes under the influence of alongshore tides if the tidal-excursion number is on the order of unity or less.

In closing, it should be noted that density and tides are not the only two forcings that affect a developing plume in the studied area. Winds are equally, if not more, important. To include winds, better parameterization of vertical viscosity may be necessary to simulate the wind-induced mixed layer. Our efforts to include winds are ongoing.

**Acknowledgments** The research is supported by grants from the National Science Council of the Republic of China under contracts NSC82-0209-M002A-008 and NSC82-0202-B-002A-012-B07.

## REFERENCES

- Chao, S.-Y., 1990: Tidal modulation of estuarine plumes. *J. Phys. Oceano.*, **20**, 1115-1123.
- Chao, S.-Y., and W. C. Boicourt, 1986: Onset of estuarine plumes. *J. Phys. Oceano.*, **16**, 2137-2149.
- Chao, S.-Y., and T. Paluszkiwicz, 1991: The hydraulics of density currents over estuarine sills. *J. Geophys. Res.*, **96**, 7065-7076.
- Eckart, C., 1958: The equation of state of water and sea water at low temperatures and pressures. *Am. J. Sci.*, **256**, 225-240.
- Garvine, R. W., 1974: Physical features of the Connecticut River outflow during high discharge. *J. Geophys. Res.*, **79**, 831-846.
- Li, C.-C., T.-H. Ts'ang, C.-H. Chang, C.-T. Chuang, L.-Y. T'sai, and K.-T. Kuo, 1991: The formation study and preliminary environmental protection design of Yin-Yang bay. Special Pub. No. 20, Center for Environmental Engineering Research, National Central University, 788pp. (in Chinese).
- Liang, S.-T., 1989: Extraction fractionation of the absorbed heavy metals in marine sediments and a case study at Lien-Tong bay, Northeast cape of Taiwan. Master thesis, Institute of Oceanography, National Taiwan University, 86pp. (in Chinese with English abstract).
- Luketina, D. A., and J. Imberger, 1987: Characteristics of a surface buoyant jet. *J. Geophys. Res.*, **92**, 5435-5447.
- Matsuno, T., and Y. Nagata, 1987: Numerical study of the behavior of heated water discharged into the ocean. Part I: the effect of Earth's rotation. *J. Oceano. Soc. Japan*, **43**, 295-308.
- O'Donnell, J., 1990: The formation and fate of a river plume: a numerical model. *J. Phys. Oceano.*, **20**, 551-568.
- Pai, S.-C., T.-C. Chen, and S.-T. Liang, 1990: Distribution of dissolved and particulate heavy metals in coastal seawater near Lian-Tong bay, northeast of Taiwan. *J. Environ. Prot. Soc.*, **13**, 19-37. (in Chinese with English abstract).
- Semtner, A. J., 1974: An oceanic general circulation model with bottom topography. Numerical Simulation of Weather and Climate, Tech. Rep. 9, Dept. of Meteorology, UCLA, 99pp.
- Wang, D.-P., 1985: Numerical study of gravity currents in a channel. *J. Phys. Oceano.*, **15**, 299-305.
- Yang, C.-Y., and J.-T. Yeh, 1990: Study on the formation of Ying-Yang Sea. *J. Environ. Prot. Soc.*, **13**, 2-7. (in Chinese with English abstract).
- Zimmerman, J. T. F., 1981: Dynamics, diffusion and geomorphological significance of tidal residual eddies. *Nature*, **290**, 549-555.